Energy Storage Materials 30 (2020) 67–73

Contents lists available at ScienceDirect

Energy Storage Materials

journal homepage: www.elsevier.com/locate/ensm

Enhanced ion conduction by enforcing structural disorder in Li-deficient argyrodites $Li_{6-x}PS_{5-x}Cl_{1+x}$

Xuyong Feng [a,1], Po-Hsiu Chien [a,c,1], Yan Wang [b], Sawankumar Patel [a], Pengbo Wang [a], Haoyu Liu [a], Marcello Immediato-Scuotto [a], Yan-Yan Hu [a,c,*]

[a] Department of Chemistry and Biochemistry, Florida State University, Tallahassee, FL, 32306, USA
[b] Advanced Materials Lab, Samsung Research America, 3 Van de Graaff Drive, Burlington, MA, 01803, USA
[c] Center of Interdisciplinary Magnetic Resonance, National High Magnetic Field Laboratory, 1800 East Paul Dirac Drive, Tallahassee, FL, 32310, USA

ARTICLE INFO

Keywords:
Solid-state lithium-ion batteries
Argyrodite fast ion conductor
$^6Li \rightarrow {}^7Li$ tracer-exchange
Ion transport pathway
Anion disorder

ABSTRACT

Solid electrolytes with high ionic conductivity and good stability are advantageous over the current liquid electrolytes in rechargeable Li-ion batteries. Argyrodites, Li_6PS_5X (X = Cl, Br, or I), with ionic conductivities on the order of mS/cm have attracted tremendous attention. However, the high potential of argyrodites in fast ion conduction is far from being reached. Significant enhancement in ion conduction relies on the fundamental understanding of the contributing factors for fast ion transport. Here, we have systematically prepared highly conductive Li-deficient $Li_{6-x}PS_{5-x}Cl_{1+x}$ and examined the influence of Li-deficiency and Cl substitution of S on ion transport using impedance spectroscopy, solid-state NMR, and first-principles calculations. With increased Cl content, the amount of Cl^- at S^{2-} (4*d*) sites increases, forming a dominant 1S3Cl (4*d*) configuration. In addition, Li^+ redistributes with significantly higher mobility. As a result, the activation energy for Li-ion transport decreases, and the conductivity increases to 17 mS/cm at 25 °C when x equals 0.7 ($Li_{5.3}PS_{4.3}Cl_{1.7}$). This work not only reports a record ionic conductivity of Cl-containing argyrodites-type fast Li-ion conductors, but also provides new insights into anion disorder-induced ion transport, which has a wide and universal appeal in the development of fast ion conductors and mixed-anion functional materials.

1. Introduction

Solid-state batteries which can provide higher energy densities, improved safety, and new chemistry by using stable solid electrolytes are the future of rechargeable batteries [1–3]. Recent advances in this area have been made to enhance ionic conductivity and stability of solid electrolytes. The ionic conductivity of solid electrolytes is related to charge carrier concentration, ion mobility, and ion transport pathways. All these factors are strongly dependent on structure and composition [4–6]. Several types of solid electrolytes with high ionic conductivity, comparable to liquid-based electrolytes, have been developed [7–11].

Among those highly conductive solid electrolytes, argyrodites (Li_6PS_5X, X = Cl, Br, and I) reported in 2008 can reach ionic conductivities on the order of 10^{-3} to 10^{-2} S/cm due to the unusually high Li^+ mobility [12]. In the past decade, the reported argyrodites (Li_6PS_5X) can reach a conductivity of several mS/cm [13–18]. The ionic conductivities of argyrodites are greatly affected by defects and disorder. In a completely ordered structure, the halide X^- ions occupy 4*a* sites (0, 0, 0) of the $F\bar{4}3m$ space group, while the free S^{2-} takes 4*d* sites (0.25, 0.25, 0.75). For X = Cl and Br, the S^{2-} (4*d*) and X^- can exchange, leading to significant disorder while this exchange rarely happens with X = I. Furthermore, the chemical nature of X also affects the Li-ion distribution in Li_6PS_5X structures at 48*h* and 24*g* sites, which greatly impacts ion conduction [12].

According to the ab initio Molecular Dynamics (AIMD) simulations [19], ordered Li_6PS_5Cl has very poor ionic conductivity (2×10^{-6} S/cm) and high activation energy (>0.5 eV). Wagemaker et al. predicted much higher conductivity of Li_6PS_5Cl with S/Cl disorder [14]. Recently, Wolfgang's group introduced Ge to replace P in Li_6PS_5I ($Li_{6+x}Ge_xP_{1-x}I$) to expand the lattice, which enhanced disorder between S and I and thus the conductivity increased significantly to a record of 18 mS/cm at room temperature [11]. However, the cost and stability of Ge will likely limit the practical application. Since the disorder between S and Cl/Br are much more significant than S/I, it should be possible to reach high

* Corresponding author. Department of Chemistry and Biochemistry, Florida State University, Tallahassee, FL, 32306, USA.
E-mail address: hu@fsu.edu (Y.-Y. Hu).
[1] These authors contributed equally to this work.

https://doi.org/10.1016/j.ensm.2020.04.042
Received 18 March 2020; Received in revised form 22 April 2020; Accepted 28 April 2020
Available online 7 May 2020

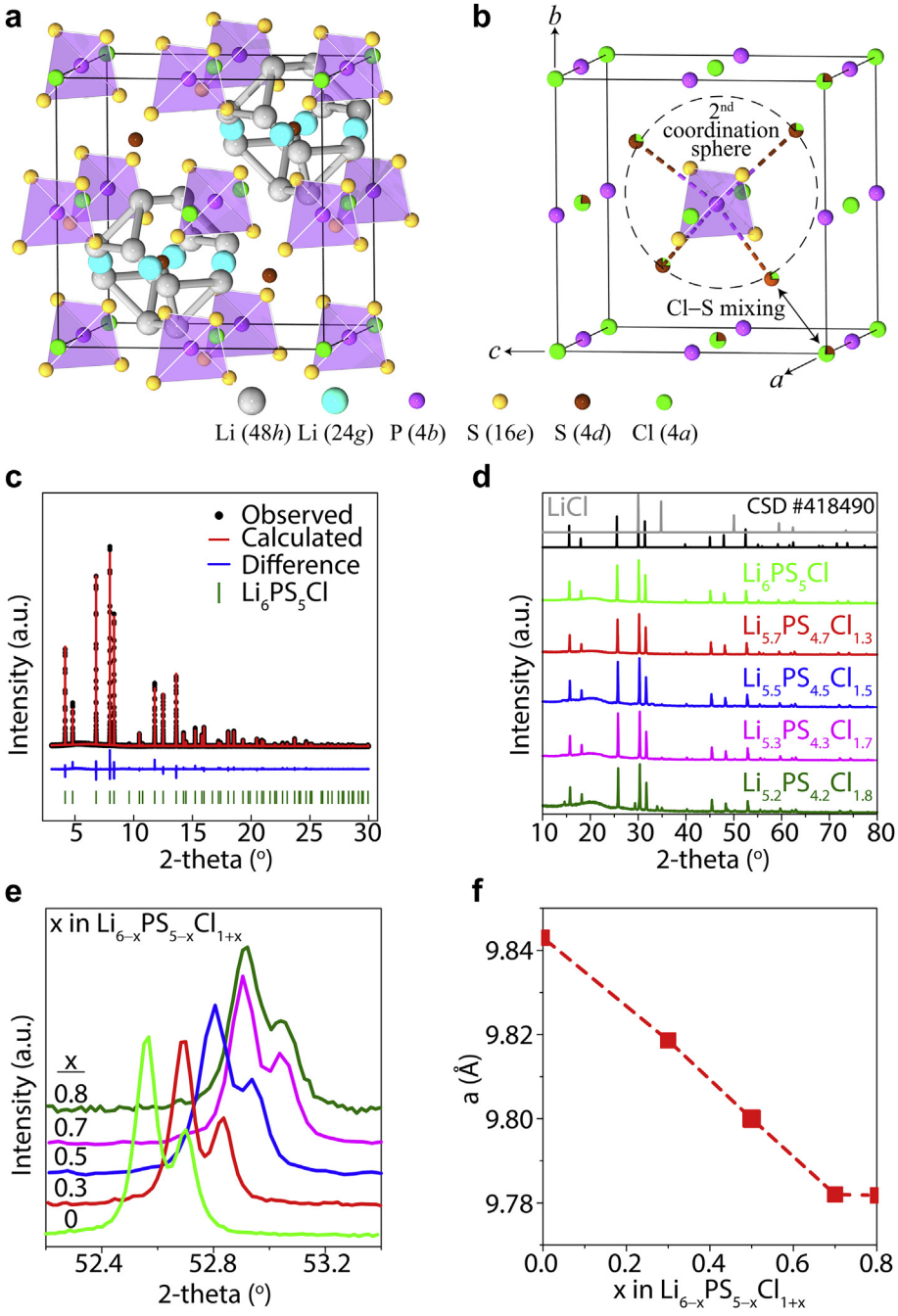

Fig. 1. (a) Crystal structure of cubic Li_6PS_5Cl ($F\bar{4}3m$) with ordered packing of Cl (Wyckoff 4*a*) and S (Wyckoff 4*d*). (b) Site disorder induced by S^{2-} (4*d*)/Cl^- (4*a*). (c) Rietveld refinement of high-resolution XRD of Li_6PS_5Cl. (d) Powder x-ray diffraction (PXRD) patterns of $Li_{6-x}PS_{5-x}Cl_{1+x}$, x = 0, 0.3, 0.5, 0.7, and 0.8. (e) Change in Bragg diffraction peaks at 52.5° and 52.7° as a function of x in $Li_{6-x}PS_{5-x}Cl_{1+x}$. (f) The lattice parameters obtained from refinement of PXRD patterns in (d) as a function of x in $Li_{6-x}PS_{5-x}Cl_{1+x}$.

conductivity in the Li_6PS_5Cl or Li_6PS_5Br system without doping Ge. Prior computational results have predicted the ionic conductivity of Li_6PS_5Cl can be over 10 mS/cm [19]. In Li_6PS_5Cl, the Cl at 4*d* site is a very important factor to Li^+ jump rate and ionic conductivity. Wagemaker et al. predicts 75% Cl at 4*d* sites gives the highest ionic conductivity [14] and reported Li_6PS_5Cl with a ionic conductivity of ~5 mS/cm at 26 °C [20]. But in the stoichiometric Li_6PS_5Cl, it is difficult to reach 75% Cl at 4*d* sites, excess Cl is needed to increase the amount of Cl at 4*d* sites. Nazar et al. reported very recently the Li-deficient $Li_{5.5}PS_{4.5}Cl_{1.5}$ with a higher conductivity of 9.4 mS/cm (12 mS/cm upon sintering) owing to increased S/Cl disorder and weakened Li-framework ion interactions [10,21].

In this work, we further the fundamental understanding of structure-ion conduction correlation with a combined experimental and computational approach. Based on more quantitative analysis of Cl occupancy, Li occupancies at 24*g* and 48*h* sites, and ion mobility as well as Li-ion transport pathways and understanding the impact of these factors on ion conduction, an ionic conductivity of 17 mS/cm at 25 °C and an activation energy of 0.22 eV have been reached with $Li_{5.3}PS_{4.3}Cl_{1.7}$.

2. Results and discussion

The Li-argyrodites, $Li_{6-x}PS_{5-x}Cl_{1+x}$ (x = 0, 0.3, 0.5, 0.7, and 0.8), are prepared to investigate the correlation of anion chemistry, structure, and composition with ionic conductivity. To create more Cl^- at 4*d* sites, beyond the limit generated by spontaneous Cl–S exchange in Li_6PS_5Cl, more Cl is inserted into the structure to replace S at the 4*d* sites with charge compensated by Li deficiency, leading to nominal compositions of $Li_{6-x}PS_{5-x}Cl_{1+x}$. Fig. 1a shows the arrangement of PS_4^{3-} tetrahedra, Cl^-, and free S^{2-} in the structure of Li_6PS_5Cl without disorder (Li ions are

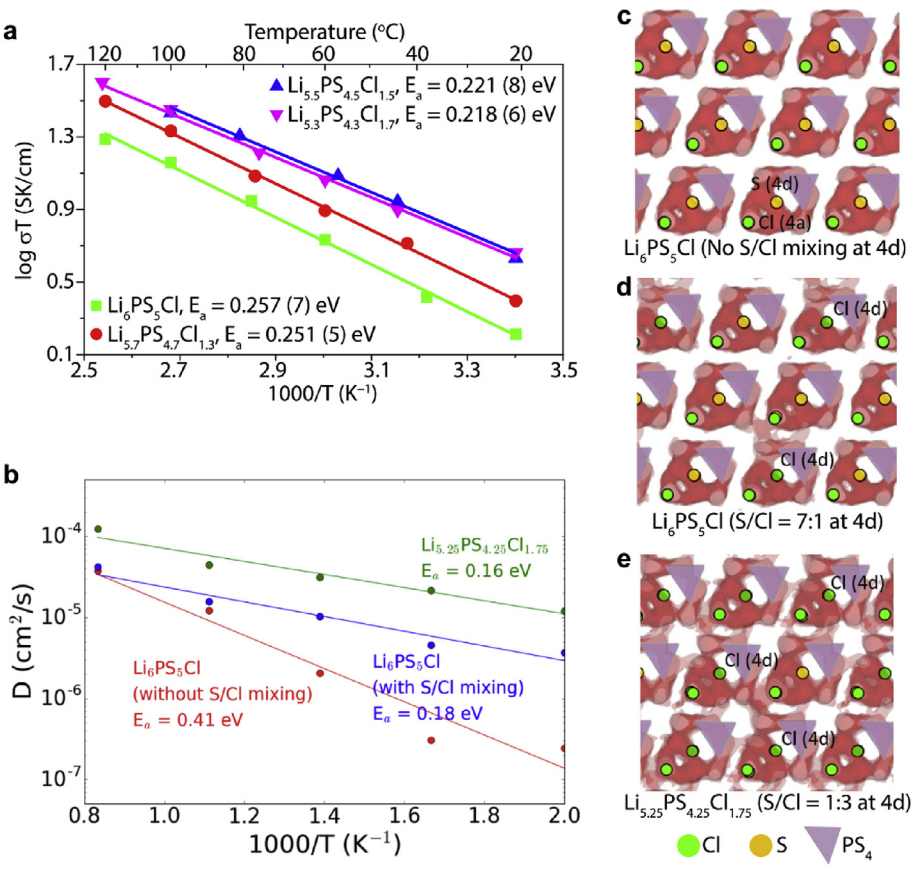

Fig. 2. Experimental measurements and AIMD calculations illustrating the impacts of S^{2-}/Cl^{-} mixing at 4*d* sites on ion conduction: (a) The Arrhenius plots of ionic conductivity as a function of temperature for $Li_{6-x}PS_{5-x}Cl_{1+x}$ (x = 0, 0.3, 0.5, and 0.7) obtained from variable-temperature impedance measurements. (b) The Arrhenius plots of Li-ion diffusivity as a function of temperature for Li_6PS_5Cl (without S^{2-}/Cl^{-} mixing at 4*d* sites), Li_6PS_5Cl (S^{2-}/Cl^{-} mixing 7:1 at 4*d*), and $Li_{5.25}PS_{4.25}Cl_{1.75}$ (S^{2-}/Cl^{-} mixing 1:3 at 4*d*) obtained from AIMD calculations. (c–e) The Li-ion probability densities of Li_6PS_5Cl (without S^{2-}/Cl^{-} mixing at 4*d* sites), Li_6PS_5Cl (with S^{2-}/Cl^{-} mixing 7:1 at 4*d* sites), and $Li_{5.25}PS_{4.25}Cl_{1.75}$ (S^{2-}/Cl^{-} mixing 1:3 at 4*d* sites). The probability densities of Li ions are obtained from AIMD simulations at 600 K with 100 ps, and the isosurfaces are plotted at isovalues of the mean value of the density. Li inside the $Li(S/Cl)_4$ tetrahedrons (48*h* sites), P (4*b* sites), and S (16*e* sites) atoms in the PS_4 tetrahedra are not shown for a clear view of the sites of interest.

omitted for clarity and the structure without Li can be found in Fig. 1b) [12], in which Cl^{-} exclusively occupies 4*a* sites, whereas free S^{2-} resides at 4*d* sites. Recent experimental evidence has revealed S^{2-}/Cl^{-} mixing at 4*d* sites (Fig. 1b) contributing to anion site disorder [22], which promotes ion conduction via an inter-cage jump mechanism. The X-ray powder diffraction patterns of $Li_{6-x}PS_{5-x}Cl_{1+x}$ (x = 0, 0.3, 0.5, 0.7, and 0.8) are shown in Fig. 1d. Preservation of structural integrity to modifications induced by varying ratios between free S^{2-} and Cl^{-} (from 1:1, 0.7:1.3, 0.5:1.5, 0.3:1.7, to 0.2:1.8) is observed, the long-range structural order stays the same as suggested by the XRD patterns with little variation (Fig. 1d). No impurities are detected up to x = 0.7, indicating that added LiCl is successfully integrated into the structures. However, unknown phases and residual LiCl are observed in nominal $Li_{5.2}PS_{4.2}Cl_{1.8}$. All the diffraction peaks continue to shift to the higher angles when doping with LiCl till x = 0.7 in $Li_{6-x}PS_{5-x}Cl_{1+x}$ (Fig. 1e), which indicates shrinkage of crystal lattice parameters (Fig. 1f), and proves the successful Cl doping with the limit of x = 0.7 ($Li_{5.3}PS_{4.3}Cl_{1.7}$).

A summary of the results from electrochemical impedance measurements on $Li_{6-x}PS_{5-x}Cl_{1+x}$ (x = 0, 0.3, 0.5, 0.7, and 0.8) are shown in Fig. S1. The ionic conductivity of $Li_{6-x}PS_{5-x}Cl_{1+x}$ positively correlates with Cl content and the highest σ of 17 mS/cm is obtained with $Li_{5.3}PS_{4.3}Cl_{1.7}$ at 25 °C. After passing the maximum Cl^{-} solubility (x = 0.7), the ionic conductivity drops along with the detection of LiCl and other impurities as seen in the PXRD when x > 0.7 in $Li_{6-x}PS_{5-x}Cl_{1+x}$. The activation energy decreases from 0.257 (±0.007) eV (x = 0) to 0.251 (±0.005) eV (x = 0.3), 0.221 (±0.008) eV (x = 0.5), and 0.218 (±0.006) eV (x = 0.7) (Fig. 2a). It is worth noting that the improvement in ionic conductivity in this work by tuning anion concentration, does not result in unwanted electronically conducting interphases, as was observed in cation doping [11,23,24].

The AIMD simulations on stoichiometric Li_6PS_5Cl and Li-deficient $Li_{5.25}PS_{4.25}Cl_{1.75}$ are performed in order to understand the effect of anion mixing in the argyrodites, and the results are shown in Fig. 2b-e. The effects of S^{2-}/Cl^{-} mixing on ion conduction are revealed by comparing the results obtained for Li_6PS_5Cl with and without S^{2-}/Cl^{-} mixing (Fig. 2b). It is found that S^{2-}/Cl^{-} mixing at 4*d* sites can lead to a much higher ionic conductivity than without S^{2-}/Cl^{-} mixing in Li_6PS_5Cl. More prominently, S^{2-}/Cl^{-} mixing significantly reduces the activation energy for ion transport (0.41 eV *vs.* 0.18 eV). The impact of Li deficiency is suggested from the comparison of results obtained for Li_6PS_5Cl with S^{2-}/Cl^{-} mixing and $Li_{5.25}PS_{4.25}Cl_{1.75}$, which shows limited change in the activation energy (0.18 eV *vs.* 0.16 eV) but nearly an order of magnitude increase in ionic conductivity. Therefore, even though Li-deficiency and S^{2-}/Cl^{-} mixing are correlated and it is challenging to completely decouple their effects on ion conduction, S^{2-}/Cl^{-} mixing seems to strongly regulate the activation energy factor for ion transport while Li-deficiency facilitates ion transport without greatly altering the energy landscape. As shown in Fig. 2c, ion diffusion is mostly isolated surrounding the S site (4*d*) in the ordered Li_6PS_5Cl without any S^{2-}/Cl^{-} mixing. When Cl^{-} occupies 4*d* sites, it induces non-localized ion conduction (Fig. 2d). The more evenly distributed probability densities of Li^{+} in $Li_{5.25}PS_{4.25}Cl_{1.75}$ (Fig. 2e) indicate a relatively flatter energy landscape than in the case of pristine Li_6PS_5Cl. Indeed, the calculated activation energy (0.16 eV) from the AIMD simulations is smaller with a much higher ionic conductivity in the $Li_{5.25}PS_{4.25}Cl_{1.75}$, which agrees very well with the results from the impedance measurements.

To gain further insights into the structural origin of fast ion conduction in $Li_{6-x}PS_{5-x}Cl_{1+x}$, we have employed a combined study of DFT structural optimization, and high-resolution $^{6,7}Li$, ^{31}P, and ^{35}Cl magic angle spinning (25 kHz) NMR to systematically investigate the effect of Cl^{-} occupancy at 4*d* sites in Li-deficient argyrodites.

The relatively flatter energy landscape in $Li_{6-x}PS_{5-x}Cl_{1+x}$ induced by S^{2-}/Cl^{-} mixing at 4*d* sites leads to the re-distribution of Li ions within the crystal structures. In the DFT optimized structure of Li_6PS_5Cl without any

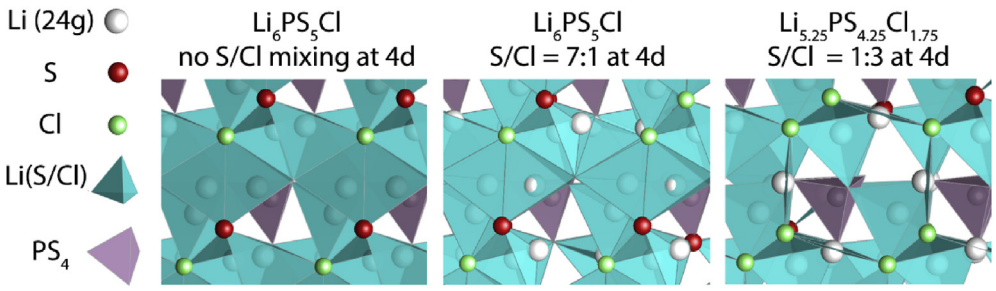

Fig. 3. Li occupancies at 24*g* and 48*h* sites in DFT optimized structures of Li_6PS_5Cl (without S^{2-}/Cl^- mixing), Li_6PS_5Cl (S^{2-}/Cl^- mixing 7:1 at 4*d*), and $Li_{5.25}PS_{4.25}Cl_{1.75}$ (S^{2-}/Cl^- mixing 1:3 at 4*d*). Li at 48*h* sites is shown in $Li(S/Cl)_4$ tetrahedra and Li at 24*g* sites is represented by white balls.

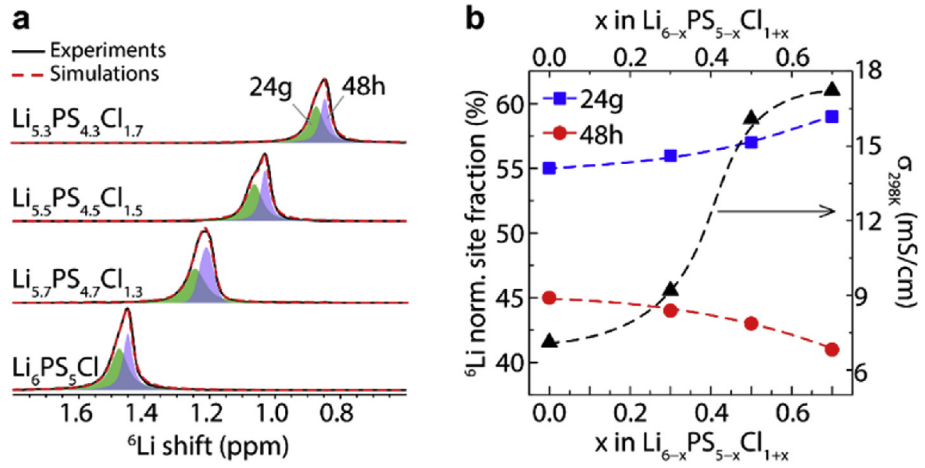

Fig. 4. Li site occupancy in $Li_{6-x}PS_{5-x}Cl_{1+x}$ (x = 0, 0.3, 0.5, and 0.7) probed by solid-state ^6Li NMR: (a) ^6Li magic-angle-spinning (MAS, 25 kHz) NMR spectra. (b) Normalized Li site fractions and ionic conductivity in $Li_{6-x}PS_{5-x}Cl_{1+x}$ (x = 0, 0.3, 0.5, and 0.7).

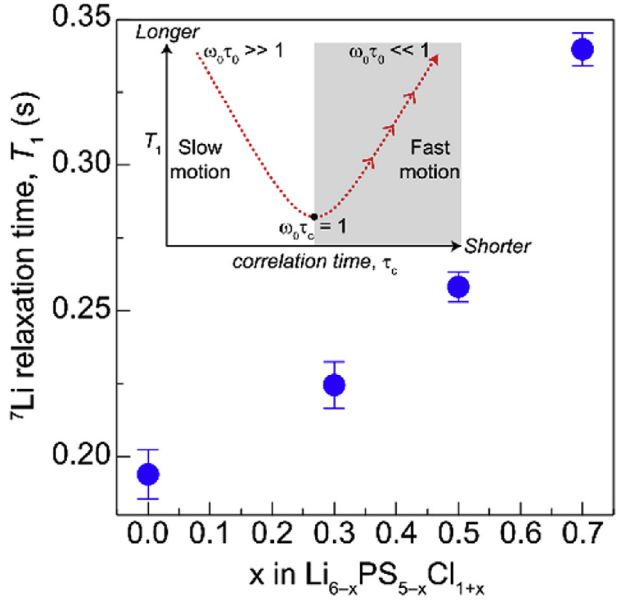

Fig. 5. ^7Li NMR T_1 relaxation time of $Li_{6-x}PS_{5-x}Cl_{1+x}$ (x = 0, 0.3, 0.5, and 0.7) as an indicator of ion mobility.

S^{2-}/Cl^- mixing, Li ions occupy only 48*h* sites, as shown in Fig. 3 [22]. In contrast, with S^{2-}/Cl^- mixing at 4*d* sites (S/Cl = 7:1) in Li_6PS_5Cl, nearly half of the Li ions are found to be displaced off 48*h* sites towards 24*g* sites, primarily due to local structural distortion caused by S/Cl disorder at 4*a* and 4*d* sites. This shift of Li ions towards 24*g* sites can also be clearly found in the Li-deficient and Cl-rich structures, for example, $Li_{5.25}PS_{4.25}Cl_{1.75}$ in Fig. 3. Furthermore, the tendency of Li occupying 24*g* sites increases with increased S^{2-}/Cl^- mixing at 4*d* sites. These DFT calculation findings echo with experimental results obtained from high-resolution ^6Li NMR as discussed in the following.

The ^6Li NMR spectra of $Li_{6-x}PS_{5-x}Cl_{1+x}$ (x = 0, 0.3, 0.5, and 0.7) are shown in Fig. 4a. Two distinct Li resonances, assigned to Li_{24g} and Li_{48h}, are identified in all $Li_{6-x}PS_{5-x}Cl_{1+x}$. In stoichiometric Li_6PS_5Cl, Li^+ can occupy both 24*g* and 48*h* sites, and the majority of Li^+ occupies more energetically favorable 48*h* sites. Li^+ at 24*g* sites is stabilized in Li-deficient $Li_{6-x}PS_{5-x}Cl_{1+x}$ due to more Li vacancies created in the Li^+ cages, and reduced repulsion between Li^+. Li occupancy at 24*g* sites contributes to shortening the inter-cage jump distances, and thus promotes long-range ion conduction. As revealed in the plots shown in Fig. 4b, a small increment in Li fraction at 24*g* sites upon the increase of x in $Li_{6-x}PS_{5-x}Cl_{1+x}$ corresponds to enhanced ionic conductivity. To quantify Li occupancies at 24*g* and 48*h* sites, the x values in nominal $Li_{6-x}PS_{5-x}Cl_{1+x}$ are first validated. The ^7Li NMR shifts of $Li_{6-x}PS_{5-x}Cl_{1+x}$ decreases linearly with increasing x (Fig. S3). Therefore, based on this linear calibration curve, the x value (x = 0, 0.3, 0.5, and 0.7) in each $Li_{6-x}PS_{5-x}Cl_{1+x}$ is confirmed. As x increases in $Li_{6-x}PS_{5-x}Cl_{1+x}$, the normalized Li^+ fraction at 24*g* sites increases. This suggests that when enhanced S^{2-}/Cl^- mixing at 4*d* sites occurs with Li deficiency, Li^+ redistributes in the lattice and favors the 24*g* sites.

As shown in Fig. 5, the ^7Li T_1 relaxation time increases with x value in $Li_{6-x}PS_{5-x}Cl_{1+x}$. Relaxation times are indicators of attempt frequency of Li^+ jumps ($\tau_{c,0}^{-1}$) in diffusional processes. Based on the Bloembergen-Purcell-Pound (BPP) model in the fast-motion region ($\omega_c\tau_c \ll 1$) [25], when ion motion increases, ^7Li T_1 times increase [26]. Therefore, the

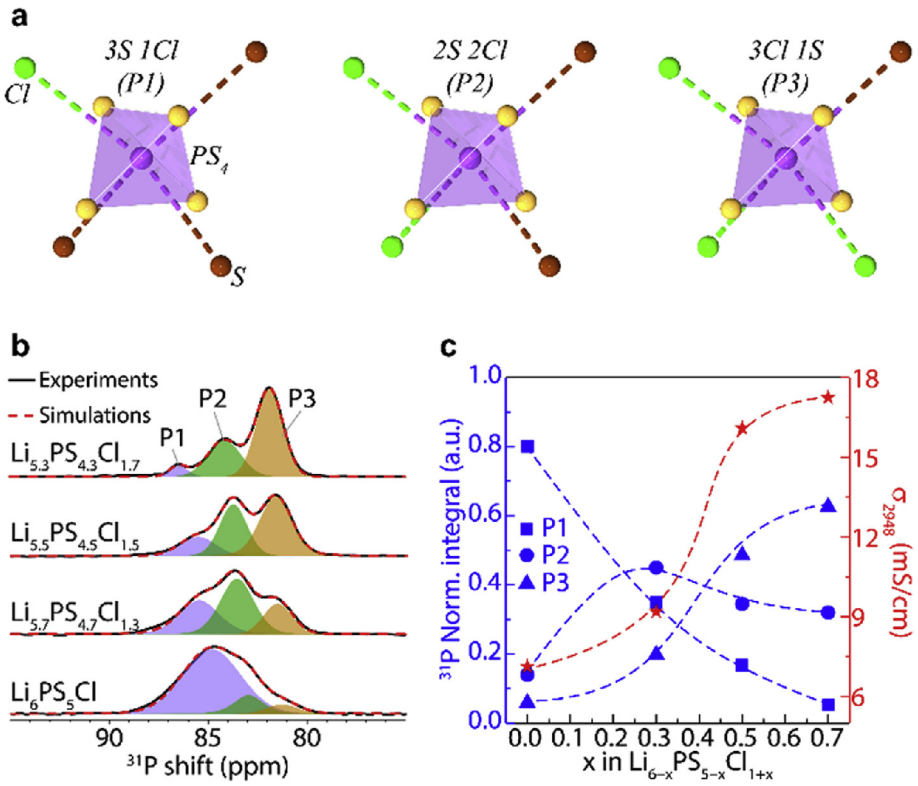

Fig. 6. (a) The schematic of distinct P environments induced by different levels of S^{2-}/Cl^{-} mixing at 4*d*/4*a* sites. (b) ^{31}P NMR spectra of $Li_{6-x}PS_{5-x}Cl_{1+x}$, x = 0, 0.3, 0.5, and 0.7. (c) The ionic conductivity and the normalized ^{31}P integral of P1, P2, and P3 NMR resonances as a function of x in $Li_{6-x}PS_{5-x}Cl_{1+x}$.

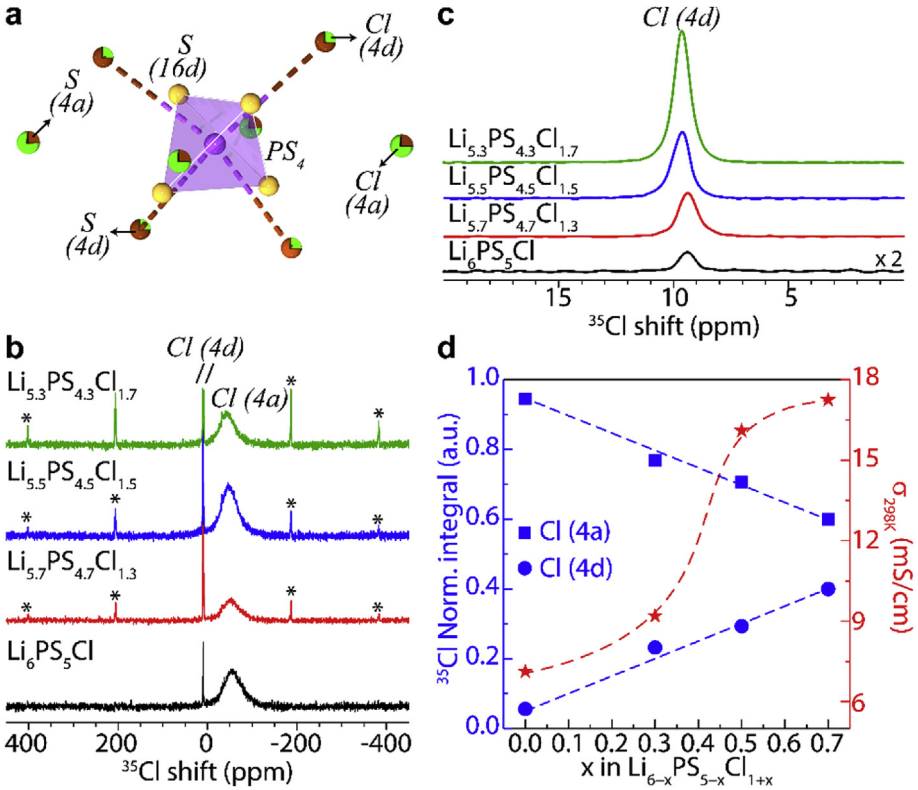

Fig. 7. (a) The schematic of S^{2-}/Cl^{-} mixing at 4*d*/4*a* sites. ^{35}Cl NMR spectra showing the Cl (4*a*) resonance (b) and the Cl (4*d*) resonance site (* denoting the spining side bands of the Cl (4*d*) resonance) (c) in $Li_{6-x}PS_{5-x}Cl_{1+x}$, x = 0, 0.3, 0.5, and 0.7. (d) The correlation of ionic conductivity with the normalized ^{35}Cl NMR integrals as a function of Cl content.

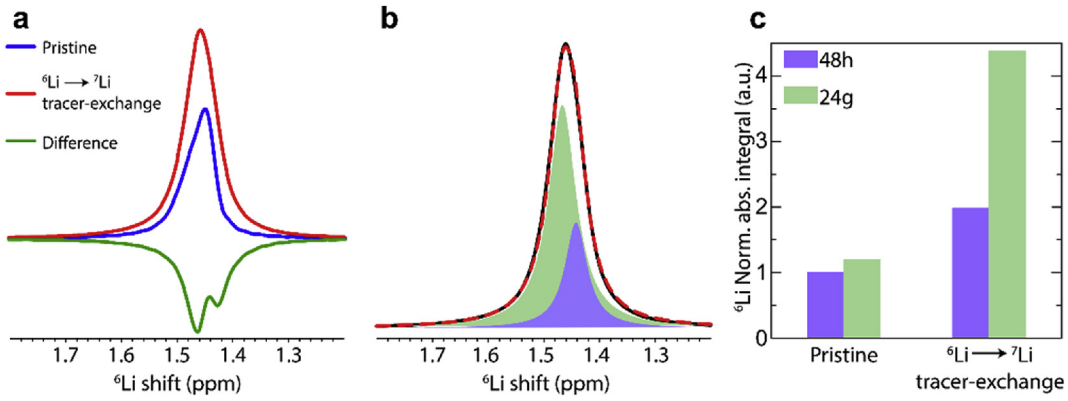

Fig. 8. Detection of ion transport pathways in Li_6PS_5Cl with $^6Li \rightarrow {}^7Li$ tracer-exchange NMR: (a) ^6Li NMR spectra before/after tracer exchange. The difference spectrum shows both Li sites are ^6Li enriched. (b) Simulation results of the ^6Li NMR spectrum after $^6Li \rightarrow {}^7Li$ tracer-exchange. Red dashed line denotes the simulation. (c) Comparisons of Li site fractions before/after $^6Li \rightarrow {}^7Li$ tracer-exchange. The ^6Li NMR integrals are normalized based on the ^6Li (48*h*) integral in pristine Li_6PS_5Cl. (For interpretation of the references to colour in this figure legend, the reader is referred to the web version of this article).

increased ^7Li T_1 NMR relaxation times suggest faster Li^+ motion as x increases in $Li_{6-x}PS_{5-x}Cl_{1+x}$. Thus, the fast ion conduction in $Li_{6-x}PS_{5-x}Cl_{1+x}$ is at least partially attributed to increased Li^+ mobility.

The S^{2-} (4*d*) locates in the secondary coordination shell of P in $Li_{6-x}PS_{5-x}Cl_{1+x}$, and S^{2-}/Cl^- mixing at 4d sites greatly affects P local structural environments, which can be quantitatively probed by ^{31}P NMR. In a completely ordered Li_6PS_5Cl structure without S^{2-}/Cl^- mixing, the Wyckoff 4*d* sites should be solely taken by S^{2-} within the second coordination sphere around the P (Wyckoff 4*b*), yielding one single ^{31}P NMR resonance. However, in experimentally obtained structures, S^{2-}/Cl^- mixing at 4*d* sites always occurs, which leads to multiple P local environments. The arrangements of S^{2-}/Cl^- atoms at four 4*d* sites surrounding P can be *4S*, *3S1Cl*, *2S2Cl*, *1S3Cl*, and 4Cl (Fig. 6a).

According to literature [22], non-mixing, i.e., the *4S* and 4Cl configurations (not shown), are not detected as both S and Cl tend to partially occupy 4*d* sites due to their similar ionic radii. ^{31}P NMR resonances (P1, P2, and P3) reflecting the three remaining possibilities of S^{2-}/Cl^- mixing are observed in $Li_{6-x}PS_{5-x}Cl_{1+x}$ (Fig. 6b). As a result, ^{31}P signals of P1, P2, and P3 sites are assigned to the P sites surrounded by *3S1Cl*, *2S2Cl*, and *1S3Cl* in the secondary coordination shell, respectively. Upon the replacement of more S^{2-} with Cl^- at 4*d* sites, P1 diminishes whereas P3 grows. On the other hand, P2 initially increases and then decreases afterwards. The quantified evolution of ^{31}P resonances as a function of x in $Li_{6-x}PS_{5-x}Cl_{1+x}$ is shown in Fig. 6c. By comparing the variation of ^{31}P NMR signals with ionic conductivity as a function of x in $Li_{6-x}PS_{5-x}Cl_{1+x}$ (Fig. 6c), we found that the amount of the P3 (*1S3Cl*) resonance is positively correlated with the improvement of ionic conductivity. This indicates that up to $x = 0.7$ in $Li_{6-x}PS_{5-x}Cl_{1+x}$, higher Cl content gives rise to the larger degree of S^{2-}/Cl^- anion site-disorder at 4*d* sites. Without producing impurities, a higher degree of anion site-disorder at 4*d* sites, promotes faster ion conduction. This experimental observation echoes with DFT MD simulation, which reveals that the *1S3Cl* configuration yields the highest Li^+ jump rates [14].

In principle, ^{35}Cl NMR is sensitive to Cl^- local structural environments, and S^{2-}/Cl^- mixing in $Li_{6-x}PS_{5-x}Cl_{1+x}$ at 4*d* sites is expected to at least produce two ^{35}Cl resonances, which correspond to Cl^- at the original 4*a* sites and the exchanged 4*d* sites (Fig. 7a).

As shown in the ^{35}Cl NMR spectra of $Li_{6-x}PS_{5-x}Cl_{1+x}$ (Fig. 7b), one sharp peak at 9 ppm and one broad signal at −25 ppm are identified. To make reliable assignments of these two ^{35}Cl resonances, ^{35}Cl NMR on lab-synthesized $Li_{5.7}PS_{4.7}Cl_{0.3}I$ are acquired (Fig. S4). In $Li_{5.7}PS_{4.7}Cl_{0.3}I$, due to the significant difference in ionic radii between I^- and Cl^-, Cl^- is expected to exclusively reside at 4*d* sites, while I^- fully occupies 4*a* sites. Thus, the major resonance found in ^{35}Cl NMR of $Li_{5.7}PS_{4.7}Cl_{0.3}I$ at 9 ppm should be from Cl^- at 4d sites. Therefore, in the ^{35}Cl NMR of $Li_{6-x}PS_{5-x}Cl_{1+x}$, the 9-ppm resonance is assigned to Cl^- at 4*d* sites while the −25 ppm one to Cl^- at 4*a* sites. The 9-ppm resonance grows with increasing x value in $Li_{6-x}PS_{5-x}Cl_{1+x}$, suggesting increased Cl^- at 4*d* sites. Furthermore, the ion dynamics of Cl^- at 4*d* sites and at 4*a* sites are remarkably different, suggested by very different ^{35}Cl T_1 NMR relaxation times. In general, a nucleus which has non-vanishing quadrupolar moment such as ^{35}Cl ($I = 3/2$) is expected to have quadrupolar couplings as the dominating NMR interaction, especially in a non-symmetric structural environment, which drives fast relaxation. In such cases, a ^{35}Cl NMR signal should observe a broad linewidth with ^{35}Cl T_1 relaxation times on the order of 10^{-3} s. However, a sharp ^{35}Cl NMR resonance and slower NMR relaxation are expected when Cl^- sites at a relatively symmetric structural environment or exhibits fast motion. An estimated ^{35}Cl T_1 time for Cl^- at 4*d* sites is 6 s, while a very short ^{35}Cl T_1 time of 0.02 s is observed for Cl^- at 4*a* sites. The short ^{35}Cl T_1 time on the order of milliseconds suggests that Cl^- at 4*a* site experiences strong quadrupolar couplings, causing a rapid dephasing of longitudinal magnetization. On the other hand, the significantly longer ^{35}Cl T_1 time on the order of seconds for Cl^- at 4*d* sites indicates fast Cl^- motion.

To identify the roles of Li sites, 24*g* or 48*h*, in fast ion conduction, $^6Li \rightarrow {}^7Li$ tracer-exchange is performed on Li_6PS_5Cl. If Li^+ ions frequently pass through certain Li sites, more ^6Li enrichment should be observed for those active Li sites. Fig. 8a presents the ^6Li NMR spectra of Li_6PS_5Cl before/after $^6Li \rightarrow {}^7Li$ tracer-exchange and the difference spectrum. No significant changes are observed in the ^{31}P NMR resonances before and after tracer-exchange (Fig. S5), suggesting that the tracer-exchange process does not alter the anion structural framework or results in any decomposition. The negative ^6Li NMR peaks in the difference spectrum indicate that the ^6Li NMR signal is enhanced after tracer-exchange. The more negative the ^6Li NMR signal is, the higher the ^6Li NMR signal of the corresponding sites is enriched. When simulating the ^6Li NMR spectrum after tracer-exchange, two resonances are found with Li_{24g} (green) showing higher intensity than Li_{48h} (purple) (Fig. 8b). This is consistent with the difference spectrum. Quantification of ^6Li NMR (Fig. 8c) before/after $^6Li \rightarrow {}^7Li$ tracer-exchange shows that ^6Li enrichment is observed for both 24*g* and 48*h* sites. The ^6Li-enrichment of 24*g* site is significantly greater. The results suggest the critical role of 24*g* sites for fast Li-ion conduction. This is consistent with the positive correlation found between enhanced ionic conductivity and increased Li occupancy at 24*g* sites.

To further decouple the roles that the Li^+ distribution and S/Cl disorder play in Li-ion conduction, we have prepared Li_6PS_5Cl at 500 °C with smaller lattice parameters and lower conductivity (Fig. S6), which is consistent with the results from literature [20]. As shown in ^6Li NMR, the fraction of Li_{24g} in Li_6PS_5Cl (500 °C) decreased (Fig. S7a) due to the shrunk lattice [12], while the magnitude of S/Cl disorder in both Li_6PS_5Cl (500 °C and 550 °C) remains nearly identical as manifested by

^{31}P NMR spectra (Fig. S7b). This result confirms the importance of Li^+ distribution (i.e., Li occupancy at 48*h* and especially 24*g* sites) to Li-ion conduction in Li-Argyrodite solid electrolytes.

3. Conclusions

In summary, we have identified a series of highly conductive Li-deficient argyrodites, $Li_{6-x}PS_{5-x}Cl_{1+x}$ (x = 0, 0.3, 0.5, and 0.7), achieving a maximum ionic conductivity of 17 mS/cm at 25 °C and a low activation energy of 0.22 eV. The detailed fundamental investigation using both experimental and computational tools has revealed that Li-deficient, Cl-rich $Li_{6-x}PS_{5-x}Cl_{1+x}$ yields high degree of S/Cl disorder, with the occupancy of Cl^- at 4*d* sites quantified by both ^{35}Cl and ^{31}P NMR. Cl^- at 4*d* sites changes Li-ion energy landscape and stabilizes Li^+ at 24*g* sites. S/Cl disorder along with lattice shrinkage in the Li-deficient structures leads to Li redistribution between 48*h* and 24*g* sites. Li-ion dynamics measurement and $^6Li \rightarrow {}^7Li$ tracer-exchange NMR also imply that Li occupancy at 24*g* sites is critical to fast ion conduction.

Declaration of competing interest

The authors declare that they have no known competing financial interests or personal relationships that could have appeared to influence the work reported in this paper.

CRediT authorship contribution statement

Xuyong Feng: Conceptualization, Methodology, Investigation, Writing - original draft. **Po-Hsiu Chien:** Conceptualization, Methodology, Investigation, Writing - original draft. **Yan Wang:** Formal analysis, Writing - original draft. **Sawankumar Patel:** Investigation. **Pengbo Wang:** Investigation. **Haoyu Liu:** Investigation, Formal analysis. **Marcello Immediato-Scuotto:** Investigation. **Yan-Yan Hu:** Conceptualization, Methodology, Investigation, Writing - review & editing, Supervision, Project administration, Funding acquisition.

Acknowledgements

The authors acknowledge the support from National Science Foundation under Grant No. DMR-1808517. All solid-sate NMR experiments were performed at the National High Magnetic Field Laboratory. The National High Magnetic Field Laboratory is supported by National Science Foundation through NSF/DMR-1644779 and the State of Florida. High resolution synchrotron XRD was carried out at Argonne National Laboratory.

Appendix A. Supplementary data

Supplementary data to this article can be found online at https://doi.org/10.1016/j.ensm.2020.04.042.

References

[1] J. Xiang, L. Yang, L. Yuan, K. Yuan, Y. Zhang, Y. Huang, J. Lin, F. Pan, Y. Huang, Alkali-Metal anodes: from lab to market, Joule 3 (2019) 2334–2363.
[2] L. Xu, S. Tang, Y. Cheng, K. Wang, J. Liang, C. Liu, Y.-C. Cao, F. Wei, L. Mai, Interfaces in solid-state lithium batteries, Joule 2 (2018) 1991–2015.
[3] B. Zhang, R. Tan, L. Yang, J. Zheng, K. Zhang, S. Mo, Z. Lin, F. Pan, Mechanisms and properties of ion-transport in inorganic solid electrolytes, Energy Storage Mater 10 (2018) 139–159.
[4] C. Yu, S. Ganapathy, E.R.H. van Eck, L. van Eijck, S. Basak, Y. Liu, L. Zhang, H.W. Zandbergen, M. Wagemaker, Revealing the relation between the structure, Li-ion conductivity and solid-state battery performance of the argyrodite Li_6PS_5Br solid electrolyte, J. Mater. Chem. A. 5 (2017) 21178–21188.
[5] Y. Wang, W.D. Richards, S.P. Ong, L.J. Miara, J.C. Kim, Y. Mo, G. Ceder, Design principles for solid-state lithium superionic conductors, Nat. Mater. 14 (2015) 1026–1031.
[6] L. Pietronero, A. Avogadro, Mechanisms of ionic conduction in glassy solid electrolytes, Solid State Ionics 3–4 (1981) 7–11.
[7] Y. Seino, T. Ota, K. Takada, A. Hayashi, M. Tatsumisago, A sulphide lithium super ion conductor is superior to liquid ion conductors for use in rechargeable batteries, Energy Environ. Sci. 7 (2014) 627–631.
[8] N. Kamaya, K. Homma, Y. Yamakawa, M. Hirayama, R. Kanno, M. Yonemura, T. Kamiyama, Y. Kato, S. Hama, K. Kawamoto, A. Mitsui, A lithium superionic conductor, Nat. Mater. 10 (2011) 682–686.
[9] Y. Kato, S. Hori, T. Saito, K. Suzuki, M. Hirayama, A. Mitsui, M. Yonemura, H. Iba, R. Kanno, High-power all-solid-state batteries using sulfide superionic conductors, Nat. Energy. 1 (2016) 16030.
[10] L. Nazar, P. Adeli, J.D. Bazak, K.-H. Park, I. Kochetkov, A. Huq, G. Goward, Boosting solid-state diffusivity and conductivity in lithium superionic argyrodites by halide substitution, Angew. Chem. Int. Ed. 58 (2019) 8681–8686.
[11] M.A. Kraft, S. Ohno, T. Zinkevich, R. Koerver, S.P. Culver, T. Fuchs, A. Senyshyn, S. Indris, B.J. Morgan, W.G. Zeier, Inducing high ionic conductivity in the lithium superionic argyrodites $Li_{6+x}P_{1-x}Ge_xS_5$ I for all-solid-state batteries, J. Am. Chem. Soc. 140 (2018) 16330–16339.
[12] H.-J. Deiseroth, S.-T. Kong, H. Eckert, J. Vannahme, C. Reiner, T. Zaiß, M. Schlosser, Li_6PS_5X: a class of crystalline Li-rich solids with an unusually high Li^+ mobility, Angew. Chem. Int. Ed. 47 (2008) 755–758.
[13] S. Boulineau, M. Courty, J.-M. Tarascon, V. Viallet, Mechanochemical synthesis of Li-argyrodite Li_6PS_5X (X=Cl, Br, I) as sulfur-based solid electrolytes for all solid state batteries application, Solid State Ionics 221 (2012) 1–5.
[14] N.J.J. de Klerk, I. Rosłoń, M. Wagemaker, Diffusion mechanism of Li argyrodite solid electrolytes for Li-ion batteries and prediction of optimized halogen doping: the effect of Li vacancies, halogens, and halogen disorder, Chem. Mater. 28 (2016) 7955–7963.
[15] C. Yu, L. van Eijck, S. Ganapathy, M. Wagemaker, Synthesis, structure and electrochemical performance of the argyrodite Li_6PS_5Cl solid electrolyte for Li-ion solid state batteries, Electrochim. Acta 215 (2016) 93–99.
[16] S. Yubuchi, S. Teragawa, K. Aso, K. Tadanaga, A. Hayashi, M. Tatsumisago, Preparation of high lithium-ion conducting Li_6PS_5Cl solid electrolyte from ethanol solution for all-solid-state lithium batteries, J. Power Sources 293 (2015) 941–945.
[17] J. Zhang, H. Zhong, C. Zheng, Y. Xia, C. Liang, H. Huang, Y. Gan, X. Tao, W. Zhang, All-solid-state batteries with slurry coated $LiNi_{0.8}Co_{0.1}Mn_{0.1}O_2$ composite cathode and Li_6PS_5Cl electrolyte: effect of binder content, J. Power Sources 391 (2018) 73–79.
[18] J. Zhang, C. Zheng, J. Lou, Y. Xia, C. Liang, H. Huang, Y. Gan, X. Tao, W. Zhang, Poly(ethylene oxide) reinforced Li_6PS_5Cl composite solid electrolyte for all-solid-state lithium battery: enhanced electrochemical performance, mechanical property and interfacial stability, J. Power Sources 412 (2019) 78–85.
[19] Z. Deng, Z. Zhu, I.-H. Chu, S.P. Ong, Data-driven first-principles methods for the study and design of alkali superionic conductors, Chem. Mater. 29 (2017) 281–288.
[20] C. Yu, S. Ganapathy, J. Hageman, L. van Eijck, E.R.H. van Eck, L. Zhang, T. Schwietert, S. Basak, E.M. Kelder, M. Wagemaker, Facile synthesis toward the optimal structure-conductivity characteristics of the argyrodite Li_6PS_5Cl solid-state electrolyte, ACS Appl. Mater. Interfaces 10 (2018) 33296–33306.
[21] L. Zhou, K.-H. Park, X. Sun, F. Lalère, T. Adermann, P. Hartmann, L.F. Nazar, Solvent-engineered design of argyrodite Li_6PS_5X (X = Cl, Br, I) solid electrolytes with high ionic conductivity, ACS Energy Lett (2018) 265–270.
[22] M.A. Kraft, S.P. Culver, M. Calderon, F. Böcher, T. Krauskopf, A. Senyshyn, C. Dietrich, A. Zevalkink, J. Janek, W.G. Zeier, Influence of lattice polarizability on the ionic conductivity in the lithium superionic argyrodites Li_6PS_5X (X = Cl, Br, I), J. Am. Chem. Soc. 139 (2017) 10909–10918.
[23] N. Minafra, S.P. Culver, T. Krauskopf, A. Senyshyn, W.G. Zeier, Effect of Si substitution on the structural and transport properties of superionic Li-argyrodites, J. Mater. Chem. A. 6 (2018) 645–651.
[24] P. Bron, B. Roling, S. Dehnen, Impedance characterization reveals mixed conducting interphases between sulfidic superionic conductors and lithium metal electrodes, J. Power Sources 352 (2017) 127–134.
[25] N. Bloembergen, E.M. Purcell, R.V. Pound, Relaxation effects in nuclear magnetic resonance absorption, Phys. Rev. 73 (1948) 679–712.
[26] V. Epp, Ö. Gün, H.-J. Deiseroth, M. Wilkening, Highly mobile ions: low-temperature NMR directly probes extremely fast Li^+ hopping in argyrodite-type Li_6PS_5Br, J. Phys. Chem. Lett. 4 (2013) 2118–2123.